JOURNAL OF SPACECRAFT AND ROCKETS
Vol. 56, No. 4, July–August 2019

Heterogeneous Surface Multisphere Models Using Method of Moments Foundations

Joseph A. Hughes* and Hanspeter Schaub†
University of Colorado, Boulder, Colorado 80309

DOI: 10.2514/1.A34434

Spacecraft can charge naturally to tens of kilovolts in geosynchronous orbit due to their interactions with the space plasma and the sun. This charging causes forces and torques that can perturb the orbits of uncontrolled debris objects. Charging is also being investigated as a form of touchless actuation in an active charging multicraft formation. The multisphere method (MSM) was recently developed to yield fast numerical approximation electrostatic forces across charged bodies. The surface MSM (or SMSM) implementation assumes a homogenous distribution of equally sized spheres across the surface. This paper details the relationship of the SMSM and the established method of moments (MOM) solution, highlighting similarities and differences. Furthermore, a new MOM-based SMSM development process is presented that allows for a heterogeneous surface sphere distribution while achieving more accurate electrostatic force evaluations as compared to prior work. Numerical examples illustrate the accuracy of the heterogeneous SMSM technique.

Nomenclature

$\boldsymbol{F}$	=	force, N
$\boldsymbol{L}$	=	torque, N/m
Q	=	charge, C
S	=	elastance, F^{-1}
V	=	voltage, V
ϵ_0	=	vacuum permittivity ($\epsilon_0 \approx 8.85418782 * 10^{-12}$), F/m
σ	=	surface charge density, C/m^2

I. Introduction

IN GEOSYNCHRONOUS Earth orbit (GEO), satellites can charge to very high voltages, sometimes as dramatic as −19 kV [1]. This charging can cause dangerous arcing as well as small forces and torques on the body due to interactions with the Earth's magnetic field, which changes the orbits of some uncontrolled lightweight debris objects through the Lorentz force [2–5]. If nearby spacecraft use active charging such as electron and ion guns, larger forces and torques are felt between the crafts. This enables novel Coulomb formation flying missions [6–8]. These forces can also be used for touchless reorbiting of GEO debris to its graveyard orbit in a matter of months using the electrostatic tractor (ET) [9–11]. If a spacecraft has a nonsymmetric charge distribution, it also experiences torques, which can be harnessed for touchless despin before servicing or grappling [12–14].

There are many separate challenges to electrostatic actuation, such as prescribing the appropriate electron and/or ion beam current and voltage; sensing the voltage, position, and attitude of a passive space object; and designing control laws that perform well for either tugging or despinning. To design and implement stable and performant control laws in any of the aforementioned mission scenarios, accurate and fast methods are needed to predict the electrostatic force and torque on both spacecraft using only in situ measurements such as the voltage of each craft, as well as their relative separation and attitude. Accuracy is important because under- or overprediction can seriously harm performance or lead to a collision [15]. The numerical evaluation speed is also important because the force and torque must be predicted in real time by the flight computer. Additionally, a faster-than-real-time evaluation allows efficient analysis before launch.

The multisphere method (MSM) is developed as a faster-than-real-time method for electrostatic force and torque prediction for conducting satellites [16]. The MSM places equipotential spheres in the body of the spacecraft, then forms a simple elastance matrix, and then solves for the charge. Once the charges are found, the force and torque can be found by applying Coulomb's law between every pair of spheres on the two spacecraft. In the volume MSM (or VMSM), the spheres are placed within the spacecraft volume, and their size and location are tuned are tuned to match the force and torque or E field predicted by a higher-fidelity truth model. The process of placing and sizing the spheres was optimized in Ref. [17]. It was found that, using only a few spheres, the force and torque can be predicted for simple spacecraft shapes within a few-percent error, even at close distances. This process was further advanced in Ref. [18] with the advancement of fitting to the predicted E field rather than the force and torque, which makes the optimization much more robust.

Another addition to the MSM family is the surface MSM (SMSM), which places equal-radius spheres equidistantly or homogeneously along the surface of the spacecraft [19]. The sphere radius is then varied so that the model matches the self-capacitance predicted by a higher-fidelity model. This model avoids nearly all of the difficulties with optimization because the sphere locations are prescribed and it is more accurate than the MSM, but it is much slower to evaluate due to the larger number of spheres. Although this SMSM performs well on certain types of shapes, there has not been a proof of convergence of this homogenous SMSM. Furthermore, this method does not allow the spheres to be more tightly packed across a particular region of interest, such as a docking surface, without increasing the sphere density throughout the entire spacecraft surface. This yields SMSMs with a large number of spheres, which slows down the numerical electrostatic force evaluation.

Although developed independently, the SMSM is very close in form to the boundary element method [20] and the method of moments (MOM), illustrated in Fig. 1. The MOM is a general numerical method that can be used to solve a variety of electromagnetic problems [21]. The MOM is similar to the SMSM, in that it inverts an elastance matrix to solve for the charge distribution but it differs in how the elastance matrix is formed. In the MSM, the elements are formed from the size and location of the spheres, which are tuned to match an externally created truth file. In the MOM, they are derived from first principles, and thus have a theoretical basis for convergence to the correct force, torque, or E fields. In this formulation, the size of the element is considered which means that each element of the elastance matrix requires a double integral. This

Received 6 November 2018; revision received 21 January 2019; accepted for publication 18 March 2019; published online 29 April 2019.

*Graduate Research Assistant, Department of Aerospace Engineering, ECEE 275, 431 UCB.

†Professor and Glenn L. Murphy Chair of Engineering, Department of Aerospace Engineering, ECNT 321, 431 UCB.

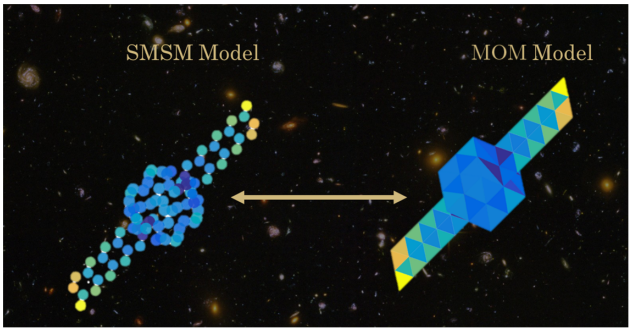

Fig. 1 Comparison between SMSM and MOM models for a template spacecraft.

nesting of a model within a model adds initial complexity, but gives a foundation for convergence. Recently, the MOM was used to estimate the capacitance of geometrically complex spacecraft and their components in Refs. [22–24]. This put an upper bound on the size of arcs that could occur. This formulation has also been applied to conductors coated with dielectrics [25].

This paper investigates the relationships between the MOM and the SMSM. This relationship is used to make SMSMs from MOM models. Because the MOM is capable of modeling general objects with nonuniform meshes, this allows for the creation of heterogeneous SMSMs for general objects. Hybrid models with some processes performed with the MOM and others performed with the SMSM are also created and are compared in their computation time and accuracy.

II. Method of Moments Formulation

A. Review of Method of Moments Formulation

The MOM for electrostatics is based on Gauss's law:

$$V(\boldsymbol{r}) = \int \frac{dq'}{4\pi\epsilon_0 \|\boldsymbol{r} - \boldsymbol{r}'\|} \tag{1}$$

where $\boldsymbol{r}$ is the observation point, and $\boldsymbol{r}'$ is the source point. The source in question is the infinitesimal charge dq, and the voltage is being observed. If the source region is discretized into area elements A_i, the voltage is

$$V(\boldsymbol{r}) = \frac{1}{4\pi\epsilon_0}\left(\int_{A_1} \frac{dA'}{|\boldsymbol{r} - \boldsymbol{r}'|}\sigma_1 + \int_{A_2} \frac{dA'}{|\boldsymbol{r} - \boldsymbol{r}'|}\sigma_2 + \ldots\right) \tag{2}$$

where σ_i is the surface charge density on the ith area element. Now, apply this equation to find the voltage of the centroid of each element to get the following matrix equation:

$$\begin{bmatrix} V_1 \\ V_2 \\ \vdots \\ V_N \end{bmatrix} = \frac{1}{4\pi\epsilon_0} \begin{bmatrix} \int_{A_1} \frac{dA}{|\boldsymbol{r}_1 - \boldsymbol{r}'|} & \cdots & \int_{A_N} \frac{dA}{|\boldsymbol{r}_1 - \boldsymbol{r}'|} \\ \int_{A_1} \frac{dA}{|\boldsymbol{r}_2 - \boldsymbol{r}'|} & \cdots & \int_{A_N} \frac{dA}{|\boldsymbol{r}_2 - \boldsymbol{r}'|} \\ \vdots & & \vdots \\ \int_{A_1} \frac{dA}{|\boldsymbol{r}_N - \boldsymbol{r}'|} & \cdots & \int_{A_N} \frac{dA}{|\boldsymbol{r}_N - \boldsymbol{r}'|} \end{bmatrix} \begin{bmatrix} \sigma_1 \\ \vdots \\ \sigma_N \end{bmatrix} \tag{3}$$

This large matrix in the center is the elastance matrix $[S]$. To match prior work in the MSM, each element in $[S]$ is divided by the area of that element to give $[S]$ units of farads^{-1} and put the charge per element $\boldsymbol{Q}$ on the right-hand side rather than the surface charge density to give the expression $\boldsymbol{V} = [S]\boldsymbol{Q}$.

B. Implementation with Triangular Elements

Next, choose triangles as the basis area and parameterize the vector $\boldsymbol{\mathcal{R}} = \boldsymbol{r}_N - \boldsymbol{r}'$. Triangles are chosen as the basis area because they are able to mesh more general shapes. To simplify $\boldsymbol{\mathcal{R}}$, consider two triangles (i and j) both formed from the corners $[\boldsymbol{A}, \boldsymbol{B}, \boldsymbol{C}]$ as shown in Fig. 2. The vectors of the form $\boldsymbol{XY}$ point from point $\boldsymbol{X}$ to point $\boldsymbol{Y}$. Now, it is clear that the separation is given by

$$\boldsymbol{\mathcal{R}} = \boldsymbol{PA} + u\boldsymbol{AB} + uv\boldsymbol{BC} \tag{4}$$

where $u, v \in [0, 1]$. The u in the uv term keeps the $\boldsymbol{BC}$ vector from going its full length near point $\boldsymbol{A}$; without it, one would integrate a parallelogram rather than a triangle. Because the triangles are not necessarily right, $\boldsymbol{AB}$ and $\boldsymbol{BC}$ are not always right and therefore the set u, v is not orthogonal. The infinitesimal area with this definition for $\boldsymbol{\mathcal{R}}$ is a trapezoid with

$$dA = u\|\boldsymbol{AB} \times \boldsymbol{BC}\| du dv \tag{5}$$

The elements of $[S]$ in this basis set are then given by

$$S_{i,j} = \frac{1}{4\pi\epsilon_0 A_j}\int_A \frac{dA}{\|\boldsymbol{\mathcal{R}}\|} = \frac{1}{4\pi\epsilon_0 A_j}\int_0^1\int_0^1 \frac{u\|\boldsymbol{AB} \times \boldsymbol{BC}\| dv du}{\|\boldsymbol{PA} + u\boldsymbol{AB} + uv\boldsymbol{BC}\|} \tag{6}$$

The denominator is expanded by dotting it with itself and then taking the square root. The first integral over v is

$$S_{i,j} = \frac{\|\boldsymbol{AB} \times \boldsymbol{BC}\|}{4\pi\epsilon_0 bcA_j}\int_0^1 \log\Bigg(bc\sqrt{u^2(ab^2 + 2\boldsymbol{AB}\cdot\boldsymbol{BC} + bc^2) + u(2\boldsymbol{PA}\cdot\boldsymbol{AB} + 2\boldsymbol{PA}\cdot\boldsymbol{BC}) + pa^2} - \log\Big(bc\sqrt{ab^2u^2 + pa^2 + 2\boldsymbol{PA}\cdot\boldsymbol{AB}u} + \boldsymbol{AB}\cdot\boldsymbol{BC}u + \boldsymbol{PA}\cdot\boldsymbol{BC}\Big)\Bigg) + \boldsymbol{AB}\cdot\boldsymbol{BC}u + bc^2u + \boldsymbol{PA}\cdot\boldsymbol{BC}du \tag{7}$$

where scalars of the form xy are the magnitude of vector $\boldsymbol{XY}$. An analytic solution to the second integral over u has not been found, and so this integral is done numerically using an adaptive quadrature algorithm. When $i = j$, there is a special form for $\boldsymbol{PA}$:

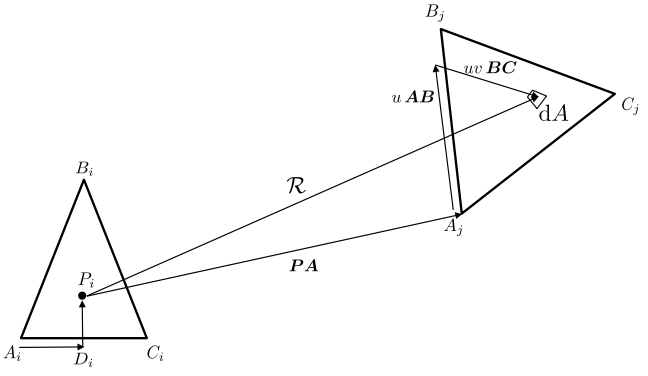

Fig. 2 Illustration of triangular coordinate system.

$$\boldsymbol{E}(\boldsymbol{P}) = \frac{\|\boldsymbol{AB}\times\boldsymbol{BC}\|Q}{4\pi\epsilon_0 A}\int_0^1\int_0^1 \frac{u^2\boldsymbol{AB}+u^2v\boldsymbol{BC}+u\boldsymbol{PA}dudv}{(u(ab^2u+2v(\boldsymbol{AB}\cdot\boldsymbol{BC}u+\boldsymbol{PA}\cdot\boldsymbol{BC})+bc^2uv^2+2\boldsymbol{PA}\cdot\boldsymbol{AB})+pa^2)^{3/2}} \tag{12}$$

where A is the area of that triangle. This is integrated over v analytically to give the following:

$$\boldsymbol{E}(\boldsymbol{P}) = \frac{-\|\boldsymbol{AB}\times\boldsymbol{BC}\|Q}{4\pi\epsilon_0 A}\int_0^1 \frac{du}{((\boldsymbol{AB}\cdot\boldsymbol{BC}u+\boldsymbol{PA}\cdot\boldsymbol{BC})^2-bc^2(u(ab^2u+2\boldsymbol{PA}\cdot\boldsymbol{AB})+pa^2))}$$
$$\left(\frac{\boldsymbol{BC}(u(u(ab^2+\boldsymbol{AB}\cdot\boldsymbol{BC})+2\boldsymbol{PA}\cdot\boldsymbol{AB}+\boldsymbol{PA}\cdot\boldsymbol{BC})+pa^2)}{\sqrt{u(u(ab^2+2\boldsymbol{AB}\cdot\boldsymbol{BC}+bc^2)+2(\boldsymbol{PA}\cdot\boldsymbol{AB}+\boldsymbol{PA}\cdot\boldsymbol{BC}))+pa^2}} - \frac{(\boldsymbol{AB}u+\boldsymbol{PA})(u(\boldsymbol{AB}\cdot\boldsymbol{BC}+bc^2)+\boldsymbol{PA}\cdot\boldsymbol{BC})}{\sqrt{u(u(ab^2+2\boldsymbol{AB}\cdot\boldsymbol{BC}+bc^2)+2(\boldsymbol{PA}\cdot\boldsymbol{AB}+\boldsymbol{PA}\cdot\boldsymbol{BC}))+pa^2}}\right.$$
$$\left. + \frac{(\boldsymbol{AB}u+\boldsymbol{PA})(\boldsymbol{AB}\cdot\boldsymbol{BC}u+\boldsymbol{PA}\cdot\boldsymbol{BC})-\boldsymbol{BC}(u(ab^2u+2\boldsymbol{PA}\cdot\boldsymbol{AB})+pa^2)}{\sqrt{u(ab^2u+2\boldsymbol{PA}\cdot\boldsymbol{AB})+pa^2}}\right) \tag{13}$$

$$\boldsymbol{PA} = -\frac{2}{3}\boldsymbol{AB}-\frac{1}{3}\boldsymbol{BC} \tag{8}$$

The integral now becomes the following:

$$S_{i,i} = \frac{1}{4\pi\epsilon_0 A_i}\int_{A_i}\frac{dA}{\mathcal{R}} = \frac{1}{4\pi\epsilon_0 A_i}\int_0^1\int_0^1 \frac{u\boldsymbol{AB}\times\boldsymbol{BC}dvdu}{\|(u-2/3)\boldsymbol{AB}+(uv-1/3)\boldsymbol{BC}\|} \tag{9}$$

The magnitude of $\mathcal{R}$ is once again found by taking the square root of the dot product of the vector with itself. The first integral over v is

$$S(i,i) = \frac{\|\boldsymbol{AB}\times\boldsymbol{BC}\|}{4\pi\epsilon_0 bcA_i}\int_0^1 \log\left(bc\sqrt{ab^2(2-3u)^2+(3u-1)(\boldsymbol{AB}\cdot\boldsymbol{BC}(6u-4)+bc^2(3u-1))}+(3u-1)bc^2+\boldsymbol{AB}\cdot\boldsymbol{BC}(3u-2)bc\right)$$
$$-\log\left(bc\sqrt{ab^2(2-3u)^2-6\boldsymbol{AB}\cdot\boldsymbol{BC}u+4\boldsymbol{AB}\cdot\boldsymbol{BC}+bc^2}-bc^2+\boldsymbol{AB}\cdot\boldsymbol{BC}(3u-2)\right) \tag{10}$$

Once again, this integral is done numerically using the adaptive quadrature algorithm. Although the function is singular when $u = 1/3$, the integral is still completed robustly. An alternative method for dealing with this singularity presented in Ref. [23] is to divide the triangle into three smaller triangles with the singularity at their common point, and then use a Duffy transformation to remove the singularity. Once this is done, the double integral is computed numerically. In contrast, the method presented here does not avoid the singularity as elegantly, but it does one of the integrals analytically. In all subsequent computations, a relative error threshold for the adaptive quadrature integrator is 10^{-3}.

These integrals can be solved analytically if the geometry is constrained and the basis area is changed from a triangle to a square in Ref. [5]. Although this gives nicer analytic solutions, squares do not mesh general shapes as well as triangles.

To validate this MOM implementation presented here, the self-capacitance of a square plate is computed with increasing resolution. The self-capacitance is shown as a function of the number of triangles in the mesh in Fig. 3a. Beginning with a mesh consisting of only two triangles, the self-capacitance is near 33 pF, and it increases up to 40.26 pF with 722 triangles for the final run. This is very close to the value from other authors using different methods [26] and involves many fewer elements than would be needed in a FEA scheme. The final charge distribution is shown in Fig. 3b. More charge accumulates at the corners of the plate, as expected.

C. *E* Field Computation

Once the charges on all the triangles have been found, the E field at an arbitrary point $\boldsymbol{P}$ is found:

$$\boldsymbol{E}(\boldsymbol{P}) = \frac{1}{4\pi\epsilon_0}\left(\int_{A_1}\frac{\sigma_1\mathcal{R}}{\mathcal{R}^3}\,\mathrm{d}A+\int_{A_2}\frac{\sigma_2\mathcal{R}}{\mathcal{R}^3}\,\mathrm{d}A+\ldots\right) \tag{11}$$

where $\mathcal{R}$ once again points from the area element to point $\boldsymbol{P}$, and dA is still $u\|\boldsymbol{AB}\times\boldsymbol{BC}\|dudv$. The E field contribution from each triangle is then as follows:

This integral over u is computed numerically because an analytic solution was not found. Keep in mind that this is the E field contribution of a single triangle. To compute the E field due to a full MOM model with many triangles, this expression must be computed for each triangle and summed. To compute the force between two models, the E field due to all triangles in the first model is computed at the centroid of each triangle in the second model and multiplied by the total charge on that triangle.

III. Multisphere Method

The multisphere method was originally created as a fast way to predict the electrostatic force and torque between conductors [16]. As shown in Fig. 4, the MSM approximates a spacecraft as a collection of spheres with variable positions and radii. It is very similar to the MOM; but, rather than the elements of the elastance matrix being derived from first principles, they are hand tuned to match the force, torque, or E fields predicted by a higher-fidelity model.

The voltage on any sphere is a function of both its own charge and the charge of all nearby spheres. If these spheres are far enough away to be approximated as point charges, the voltage is given by [16] the following:

$$V_i = \frac{1}{4\pi\epsilon_0}\frac{Q_i}{R_i}+\sum_{j=1,j\neq i}^{n}\frac{1}{4\pi\epsilon_0}\frac{Q_j}{r_{i,j}} \tag{14}$$

where q_i and R_i are the charge and radius of the ith sphere, respectively; $r_{i,j}$ is the center-to-center distance between spheres i and j; and ϵ_0 is the permittivity of the free space constant. If the voltages of each sphere are given by $\boldsymbol{V} = [V_1, V_2, \ldots, V_n]^T$ and the charges are given by $\boldsymbol{Q} = [Q_1, Q_2, \ldots, Q_n]^T$, the relationship between the two is

$$\boldsymbol{V} = [S]\boldsymbol{Q} \tag{15}$$

where $[S]$ is the elastance matrix defined as follows:

$$[S] = \frac{1}{4\pi\epsilon_0}\begin{bmatrix} 1/R_1 & 1/r_{1,2} & \cdots & 1/r_{1,n} \\ 1/r_{2,1} & 1/R_2 & \cdots & 1/r_{2,n} \\ \vdots & \vdots & \ddots & \vdots \\ 1/r_{n,1} & 1/r_{n,2} & \cdots & 1/R_n \end{bmatrix}\begin{bmatrix} Q_1 \\ Q_2 \\ \vdots \\ Q_n \end{bmatrix} \tag{16}$$

If the voltage is known, the linear system can be solved for the charges $\boldsymbol{Q}$. In either the MSM or MOM, if there are two charged conducting bodies, this matrix takes on a block form:

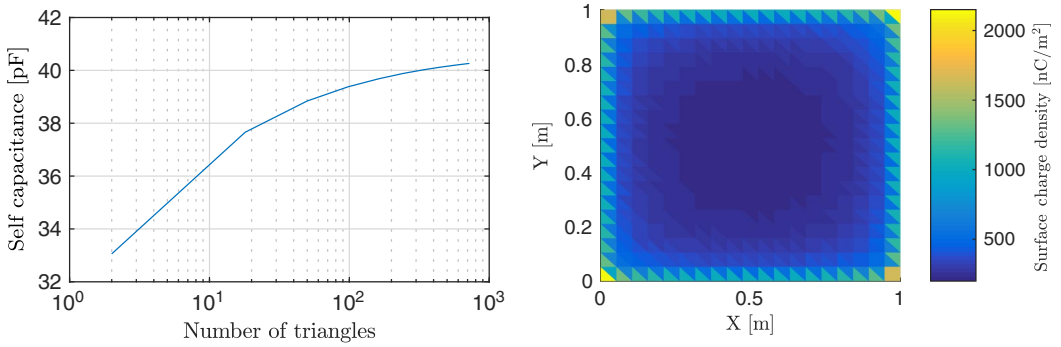

a) Self capacitance as a function of number of triangles used

b) Charge distribution for a square plate charged to 10 kV

Fig. 3 Validation of MOM implementation on a square plate.

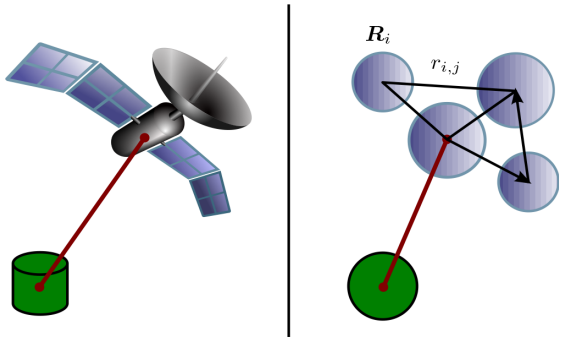

Fig. 4 Multisphere method concept.

$$\begin{bmatrix} \boldsymbol{V}_1 \\ \boldsymbol{V}_2 \end{bmatrix} = \begin{bmatrix} S_1 & S_M \\ S_M^T & S_2 \end{bmatrix} \begin{bmatrix} \boldsymbol{Q}_1 \\ \boldsymbol{Q}_2 \end{bmatrix} \tag{17}$$

where S_M and S_M^T are the mutual blocks of the elastance matrix, and S_1 and S_2 are the diagonal blocks. To find the E field from a charged spacecraft at point $\boldsymbol{r}_i$, sum the contributions from each MSM sphere. This is shown for body 1, which has m spheres in its MSM model:

$$\boldsymbol{E}_1(\boldsymbol{r}_i) = \frac{1}{4\pi\epsilon_0} \sum_{j=1}^{m} \frac{\boldsymbol{Q}_{1_j} \boldsymbol{r}_{i,j}}{r_{i,j}^3} \tag{18}$$

where $\boldsymbol{r}_{i,j}$ points from sphere j in body 1 to point $\boldsymbol{r}_i$. To find the force and torque on another body, sum the product of the E field and the charge over the second body. This is shown for body 2, which has an MSM model with n spheres:

$$\boldsymbol{F}_2 = \sum_{i=1}^{n} \boldsymbol{Q}_{2_i} \boldsymbol{E}_1(\boldsymbol{r}_i) \tag{19}$$

$$\boldsymbol{L}_2 = \sum_{i=1}^{n} \boldsymbol{Q}_{2_i} \boldsymbol{r}_i \times \boldsymbol{E}_1(\boldsymbol{r}_i) \tag{20}$$

The MSM divides into the volume MSM and the surface MSM. In the VMSM, a few spheres are placed inside the volume of the object; and, in the SMSM, the spheres are placed uniformly on the surface of the object. Although the VMSM requires both the size and location of the spheres to be optimized to match an external truth file, the SMSM sizes the spheres to match the externally computed self-capacitance and does not need any optimization. For rectangular planar surfaces, placing the spheres uniformly is done easily using grids. In Ref. [18], this was done using MATLAB's meshgrid function. These rectangles are assembled to make template box and panel spacecraft with minimal effort. Stevenson and Schaub [19] used a golden spiral algorithm to distribute points on a sphere and cylinder, but there was uncertainty about the transition from the body of the cylinder (which used hexagonal packing) to the circular endcaps (which used a golden spiral). Additionally, although canonical shapes such as spheres, rectangular plates, and circular plates have closed-form answers that are easy to implement, extending the homogeneous SMSM to general spacecraft geometries is an unsolved problem.

IV. Comparison Between MSM and MOM

The MSM and MOM both place elements on the surface of the conductor and then use an elastance matrix to solve for the charge distribution. They differ in how they make the elements of the elastance matrix. With the MOM, this is done using a double integral of one over the distance from the observation point to a source point in the other element. In the MSM, it is one over the distance between the centroids. This is shown schematically in Fig. 5.

The MSM approximates the integrals of $1/\mathcal{R}$ as either one over the radius of that sphere or one over the distance to the other sphere. The center-to-center distance is similar to the vector $\boldsymbol{PA}$, which is the largest term in the denominator. The radius of the sphere is similar to the effective radius of the triangular element. Once again, the MSM spheres are positioned and sized to match the force, torque, or E fields computed from a higher-fidelity model so that the elements of the elastance matrix have limited physical or geometric significance.

To better understand how the MOM triangular element compares to the MSM sphere, consider a constant-area isosceles MOM

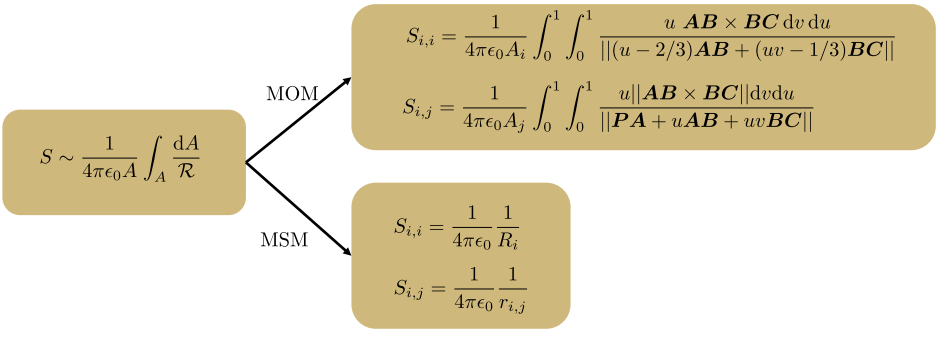

Fig. 5 Differences between MOMs and MSMs.

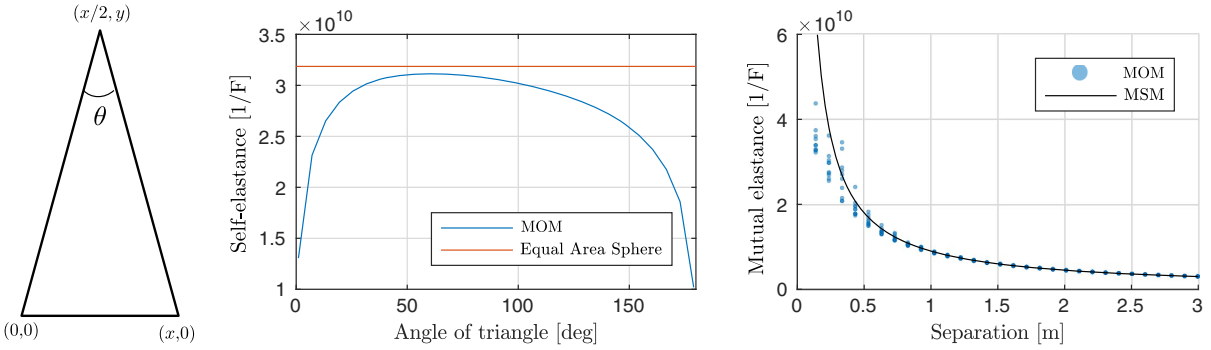

a) MOM triangle **b) Self-elastance for a MOM triangle and a MSM sphere** **c) Mutual elastance for MOM triangles and MSM spheres**

Fig. 6 Comparison of MOM and MSM elements.

triangle, shown in Fig. 6a. When θ is small, the triangle is very tall and skinny; when $\theta = 60$ deg, the triangle is equilateral; and when θ is near 180 deg, it becomes very obtuse. The self-elastance is plotted as a function of θ along with the constant self-elastance of a MSM sphere with the same area ($R = \sqrt{A/4\pi}$) in Fig. 6b. The assumption of equal area is often a very good assumption, especially for convex shapes [27]. This assumption was used in Ref. [28] to calculate the self-capacitance of many varied spacecraft shapes. The elastance of the triangle is very small when it is either very obtuse or very acute, and it reaches a maximum when the angle is 60 deg. This is because $\mathcal{R}$ takes on larger values when the triangle is long and skinny in either limit, although the elastance is smaller for a very obtuse triangle than for a very acute one. The effective sphere always overestimates the self-elastance if computed on the basis of equal area, and this is exaggerated for very acute or obtuse triangles.

Next, consider the mutual elastance. For two MSM spheres, it is simply given by $1/4\pi\epsilon_0 d$, where d is the separation between the centroids. For two MOM triangles, it is the double integral over the area, and is therefore attitude dependent. To investigate this, one equilateral triangle is held with its centroid at the origin but has its attitude free, whereas another identical triangle moves along the z axis and stays parallel to the x, y plane. The mutual elastance for this pair of triangles is shown alongside the mutual elastance for a pair of spheres with the same centroid separation in Fig. 6c. Special care is taken to ensure that the bottom triangle does not rotate so far that it intersects the upper triangle when the two triangles are close. The triangles both have all side lengths equal to 1 m and have their centroids on the z axis. For very close separations, the MSM is a little higher than the mean MOM solution, but for distances on the order of the edge length or greater, the MSM agrees very well with the MOM average and the MOM variation becomes very small. This is because, as vector $\boldsymbol{PA}$ gets larger and larger, the small u and v terms matter less in Eq. (6). This shows that the MSM and MOM have negligible differences when computing the mutual elastances but significant differences when computing the self-elastances.

V. MOM-Inspired MSMs

To make a MSM model from a MOM model, the mutual terms do not need to be used because the MSM solution matches them quite well using the centroid assumption. However, the radii of the MSM spheres do not match well using the equal area assumption, and there is a lot of sensitivity to the type of triangle. Therefore, a mapping is created to find the radius of the MSM sphere that will match the diagonal in the MOM elastance matrix:

$$R_i = \frac{1}{4\pi\epsilon_0 S_{i,i}} \tag{21}$$

Spheres with this radius are placed at the centroid of each triangle to create the SMSM. In prior work, all SMSM spheres had a homogeneous radius, and it was varied in order to match self-capacitance [19]. This new approach allows for heterogeneous radius SMSMs to be created. This process is illustrated on a homogeneous case where all MOM triangles (and therefore all SMSM spheres) are the same and on two heterogeneous cases where the MOM triangles are not the same size in Fig. 7.

The top row in Fig. 7 shows three different MOM models for increasingly more complicated geometries. The first model (Fig. 7a) is a square plate with 50 identical triangular elements. The resulting SMSM is shown in Fig. 7d. Although only the diagonal terms in the elastance matrix are matched, the self-capacitances only differ by 0.3%. Homogeneous SMSMs for rectangular plates have been created before using the old method of varying the radius to match the known self-capacitance [18]. Using the MOM to compute the sphere radii is done for continuity in this case.

The next plot (Fig. 7b) shows a more complex geometry of a cylinder. This mesh is not uniform due to the circular endcaps, where some triangles to have different areas and angles than the others. The area of the elements varies from 0.013 to 0.024 m^2, with the smallest triangle being at the very center. The resulting heterogeneous SMSM is shown in Fig. 7e, and the radii in this model vary from 3.3 to 4.5 cm. These two models only differ by 0.14% in self-capacitance. Homogeneous models for the cylinder have also been created before [19], but there was always some uncertainty about how to place spheres at the intersection between the circular endcaps and the main cylinder. Using the MOM removes this uncertainty because the location and size of the spheres are found from the MOM model.

The last model, shown in Fig. 7c, is a stereolithography file of a buffalo[‡] that has been downsampled. This model provides a complex surface geometry with both broad and narrow features. This model has 744 triangles, with the largest triangle's area more than 200 times as large as the smallest. The resulting MSM model is shown in Fig. 7f, and the self-capacitances only differ by 0.1%. This complex of a shape would have been impossible to model with the SMSM using prior methods, but it is easy using the MOM. These three examples show how MSM models can be created from general MOM models. Because this version of the MOM uses a triangular basis set, it can be applied to general stereolithography files, which allows for a wide array of objects, such as the buffalo shown in Fig. 7c.

VI. Two-Body Force and Torque

Close-proximity electrostatic tugging is one driver of the need for accurate and fast electrostatic solvers, and so this section compares the MOM to SMSM for the electrostatic tractor [9–11]. The tug craft is modeled as a 1 m cube with two 2×1 m solar panels charged to $+30$ kV and is located at $\boldsymbol{r} = [5, 2, 1]^T$, which puts it at a center-to-center distance of 5.48 m away from the origin; although, for some attitudes, the solar panels can come much closer. The debris object is a 3×1 m cylinder model of a spent rocket stage; it is held at the origin and charged to -30 kV. In most ET applications, the standoff distance is a more conservative 10–50 m, and so this case represents one of the most challenging examples of electrostatic force and

[‡]Data available online at https://www.thingiverse.com/thing:726062.

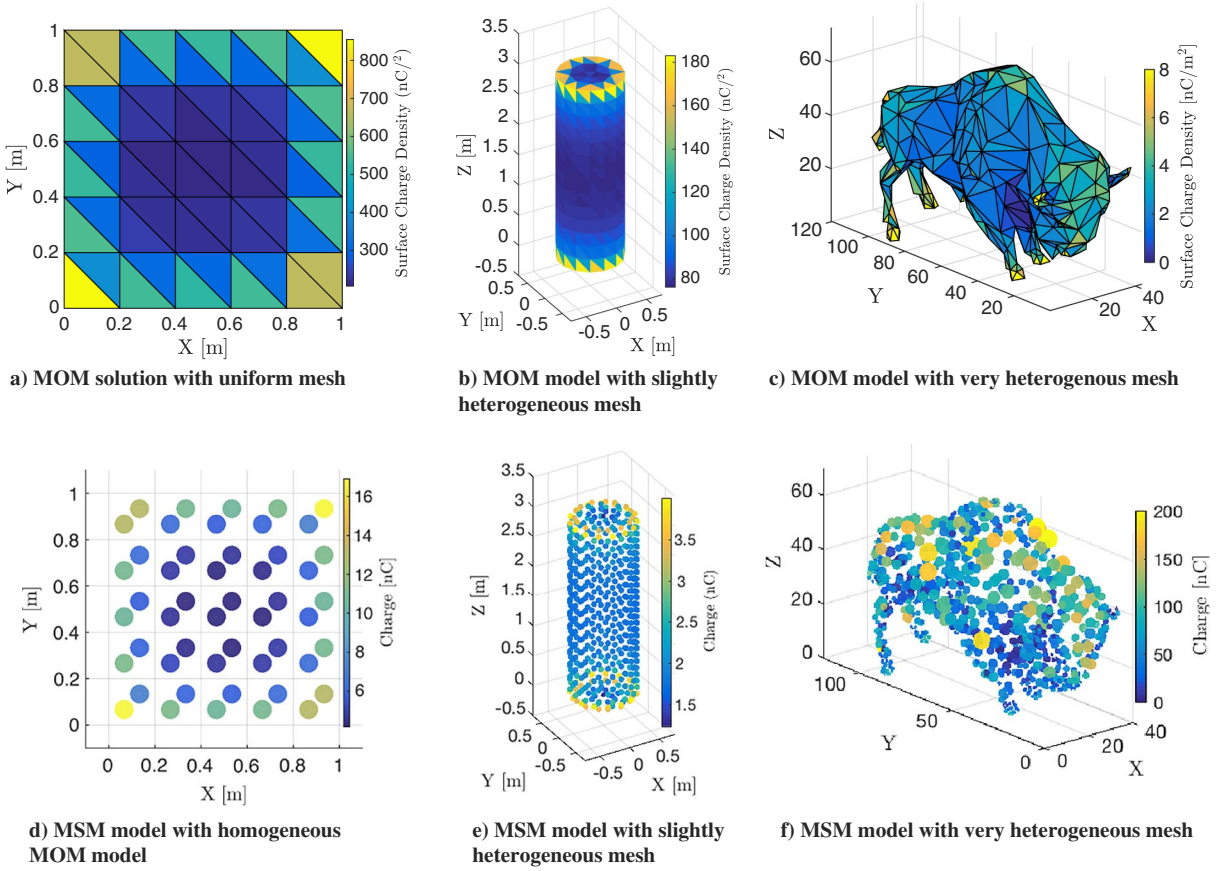

a) MOM solution with uniform mesh

b) MOM model with slightly heterogeneous mesh

c) MOM model with very heterogenous mesh

d) MSM model with homogeneous MOM model

e) MSM model with slightly heterogeneous mesh

f) MSM model with very heterogeneous mesh

Fig. 7 MSM models created from MOM models. Voltage is 10 kV in all plots.

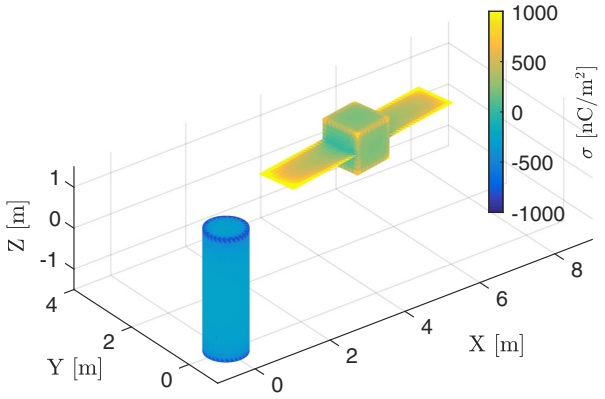

Fig. 8 High-fidelity MOM truth model for close-proximity electrostatic tugging.

torque prediction. The truth model for this situation is taken as a very high-resolution (10 cm) MOM model, which uses 2100 elements for the cylinder and 1656 elements for the tug; it is shown in Fig. 8. The color scale is capped at 1000 $\mathrm{nC/m^2}$ in this plot, but the actual charge density goes up to almost 4000 $\mathrm{nC/m^2}$ at the corners of the solar panels. Because the electrostatic solution is highly attitude dependent, the force and torque on the cylinder are computed at 16 representative tug attitudes and stored in a master text file. For each of the 16 attitudes, more than 1.7 million numerical integrals are done to make the elastance matrix. Then, this 3756×3756 matrix is inverted to solve for the charge on each element. Finally, almost 3.5 million numeric integrals are done to find the force and torque on both bodies. This process takes nearly two days on a standard laptop.

Once the truth model is created, the force and torque are computed using lower-fidelity MOMs and SMSMs while keeping track of the computation time. There are many modifications that can be made to both the MOM and SMSM to make them faster and more accurate for the ET case that are also analyzed along with the standard ones. First, because both the tug and debris are assumed to be rigid bodies, the two diagonal blocks in the elastance matrix shown in Eq. (17) do not change and do not need to be recomputed at each time step. Second, the offdiagonal blocks can be computed with the SMSM using the centroid assumption, even if the diagonal blocks are made using the MOM. The offdiagonal blocks can also not be counted at all, which ignores all induced effects. The force and torque can be computed with either the MOM or the SMSM as well. Finally, a pure SMSM can have all its sphere radii varied to match the self-capacitance of the truth model rather than from the MOM model that created it. This method works best for the homogeneous and near-homogeneous MOM models because all MSM spheres end up the same size. In all, seven different MOM/SMSM hybrid models are analyzed for this case. The name of each one and what makes it unique are shown in Table 1.

For each model variant, the mesh is computed with either 258, 500, 830, 1236, or 1730 total elements and then compared to the truth model made with 3756 elements at each of the 16 attitudes. The performance of all seven model variants is shown in Fig. 9. The error is computed as

$$\text{Error} = \frac{1}{2}\left(\frac{\|\boldsymbol{F}-\boldsymbol{F}_T\|}{\|\boldsymbol{F}_T\|}+\frac{\|\boldsymbol{L}-\boldsymbol{L}_T\|}{\|\boldsymbol{L}_T\|}\right) \tag{22}$$

where $\boldsymbol{F}$ and $\boldsymbol{L}$ are the predicted force and torque, and $\boldsymbol{F}_T$, $\boldsymbol{L}_T$ are the true force and torque. The execution time is found using MATLAB's tic and toc functions. Despite the same math being performed, the execution time varies considerably. This variance would likely disappear, and the overall time would decrease substantially on a more flight-computer-like system. Each dot in Fig. 9 represents the error and time for a different model variant with a different number of elements at different attitude. The model variant is indicated by the color in the figure legend. The number of elements is shown by

Table 1 MOM and SMSM variants used

Name	Diagonal blocks	Offdiagonal blocks	E field	Notes
Full MOM	MOM	MOM	MOM	— —
Fast MOM	MOM	SMSM	MOM	Executes in about 80% of full MOM time
Faster MOM	MOM	MOM	SMSM	Executes in about 20% of full MOM time
Fastest MOM	MOM	SMSM	SMSM	Executes in less than 1% of full MOM time
Self-MOM	MOM	0	SMSM	No induced effects included
SMSM	SMSM	SMSM	SMSM	— —
Tuned SMSM	SMSM	SMSM	SMSM	Sphere radius tuned to match C_S

grouping: each shaded group of points has the same number of elements. Lines of the same color trace the means of both the error and execution time for each model variant. As the number of elements increases, the error drops and the execution time increases: the groups of points with 258 elements are in the upper left corner of the plot, and the groups with 1730 total elements are in the bottom right.

The full MOM performance is shown in dark blue and is furthest to the right, which means it is the slowest. If the number of elements is increased up to 3756, it would have exactly 0% error because that is how the truth model is made. Even with a relatively small (258) number of elements, the error is still below 10%, even at this very close separation. The next model variant is the fast MOM, which uses the SMSM approximation for the offdiagonal blocks of the elastance matrix. This simplification does not introduce significant errors, but it saves a considerable (20%) amount of computation time. The next variant is the faster MOM, which uses the SMSM approximation for the E field but not for the offdiagonal blocks. This also does not introduce significant errors but saves a lot (80%) of computation time. The next variant is the fastest MOM, which uses the SMSM for both the offdiagonal blocks and the E field. This variant runs very fast when compared to the full MOM solution and only gives up a very small amount of accuracy. The last MOM variant is the self-MOM, which does not include any induced effects. Because of this, there are no mutual terms to compute and it runs the fastest of any model. However, it also has the worst errors (∼40%) of any model. This shows just how important the mutual interaction is at this close distance. Further away, these errors would drop considerably. The next model is the SMSM, which is almost identical to the fastest, MOM in both time and accuracy. However, the fastest MOM is slightly faster and more accurate, especially with a small number of elements. The last model variant is the tuned SMSM. This model uses the centroids from the MOM model but uniformly sizes all spheres in order to match the self-capacitance found from the truth model. This homogeneity introduces small errors for the cylinder, which does not have a uniform MOM mesh. Despite this, the tuned SMSM is by far the most accurate, being almost an order of magnitude more accurate than any other model with the same number of elements.

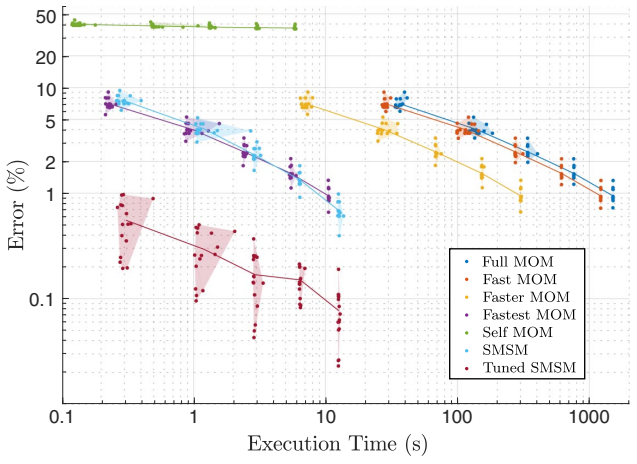

Fig. 9 Time and error shown for different force and torque prediction schemes.

VII. Conclusions

This paper analyzes the relationships between the method of moments and the multisphere method, and it uses this information to make better multisphere method (MSM) models. This is done by implementing the method of moments (MOM) using triangular elements and finding semianalytic expressions for the elastance matrix elements. Then, a mapping is created from the diagonal elements of this elastance matrix that sizes the surface MSM (or SMSM) spheres, which are placed at the centroids of the MOM triangles. This mapping allows the SMSMs to be made for general objects using triangular meshes. Different SMSM and MOM models are compared in their accuracy and computation times, and a tuned SMSM with spheres adjusted to match the true self-capacitance is found to be the most accurate.

This work shows that the MOM and MSM are very closely related methods with different approaches to solving the same integrals, illustrated in Fig. 5. A better understanding of how the MOM is formulated lends insight to the MSM and allows more complex heterogeneous surface sphere models to be created. The newly tuned SMSM can better approximate the electrostatic force for general spacecraft shapes, and it yields the capability to have an uneven surface sphere density to reduce the total number of spheres required while increasing the accuracy.

Acknowledgments

This work is supported by the U.S. Air Force Office of Scientific Research grant number FA9550-15-1-0407. Thanks go to Miles Bengtson, Kieran Wilson, and Jordan Maxwell for fruitful research conversations.

References

[1] Olsen, R. C., "The Record Charging Events of ATS-6," *Journal of Spacecraft and Rockets*, Vol. 24, No. 4, 1987, pp. 362–366. doi:10.2514/3.25925

[2] Früh, C., Ferguson, D., Lin, C., and Jah, M., "The Effect of Passive Electrostatic Charging on Near-Geosynchronous High Area-to-Mass Ratio Objects," *Proceedings of the AAS Space Flight Mechanics Meeting*, Santa Fe, NM, Feb. 2014, pp. 3121–3137, https://www.space-flight.org/docs/2014_winter/2014_winter.html.

[3] Hughes, J., and Schaub, H., "Rapid Charged Geosynchronous Debris Perturbation Modeling of Electromagnetic Disturbances," *Journal of Astronautical Sciences*, Vol. 65, No. 2, June 2018, pp. 135–156.

[4] Paul, S. N., and Früh, C., "Space-Object Charging and Its Effect on Orbit Evolution," *Journal of Guidance, Control, and Dynamics*, Vol. 40, No. 12, 2017, pp. 3180–3198.

[5] Hughes, J., and Schaub, H., "Space Weather Influence on Electromagnetic Geosynchronous Debris Perturbations Using Statistical Fluxes," *AGU Space Weather*, Vol. 16, No. 4, 2018, pp. 391–405. doi:10.1002/swe.v16.4

[6] Berryman, J., and Schaub, H., "Analytical Charge Analysis for Two- and Three-Craft Coulomb Formations," *Journal of Guidance, Control, and Dynamics*, Vol. 30, No. 6, Nov.–Dec. 2007, pp. 1701–1710. doi:10.2514/1.23785

[7] Hogan, E., and Schaub, H., "Collinear Invariant Shapes for Three-Craft Coulomb Formations," *Acta Astronautica*, Vol. 72, March–April 2012, pp. 78–89. doi:10.1016/j.actaastro.2011.10.020

[8] Inampudi, R., and Schaub, H., "Optimal Reconfigurations of Two-Craft Coulomb Formation in Circular Orbits," *Journal of Guidance, Control, and Dynamics*, Vol. 35, No. 6, Nov.–Dec. 2012, pp. 1805–1815. doi:10.2514/1.56551

[9] Bengtson, M., Wilson, K., Hughes, J., and Schaub, H., "Survey of the Electrostatic Tractor Research for Reorbiting Passive GEO Space Objects," *Astrodynamics*, Vol. 2, No. 4, Dec. 2018, pp. 291–305. doi:10.1007/s42064-018-0030-0

[10] Hughes, J., and Schaub, H., "Electrostatic Tractor Analysis Using a Measured Flux Model," *The 15th Spacecraft Charging Technology Conference*, Kobe, Japan, June 2018.

[11] Schaub, H., and Moorer, D. F., "Geosynchronous Large Debris Reorbiter: Challenges and Prospects," *Journal of the Astronautical Sciences*, Vol. 59, Nos. 1–2, 2014, pp. 161–176.

[12] Bennett, T., and Schaub, H., "Touchless Electrostatic Three-Dimensional Detumbling of Large Axi-Symmetric Debris," *Journal of Astronautical Sciences*, Vol. 62, No. 3, 2015, pp. 233–253.

[13] Bennett, T., Stevenson, D., Hogan, E., McManus, L., and Schaub, H., "Prospects and Challenges of Touchless Debris Despinning Using Electrostatics," *Advances in Space Research*, Vol. 56, No. 3, 2015, pp. 557–568. doi:10.1016/j.asr.2015.03.037

[14] Bennett, T., and Schaub, H., "Capitalizing on Relative Motion in Electrostatic Detumbling of Axi-Symmetric Geo Objects," *6th International Conference on Astrodynamics Tools and Techniques (ICATT)*, Darmstadt, Germany, March 2016, Paper 141, https://indico.esa.int/event/111/contributions/402/contribution.pdf.

[15] Hogan, E., and Schaub, H., "Relative Motion Control for Two-Spacecraft Electrostatic Orbit Corrections," *Journal of Guidance, Control, and Dynamics*, Vol. 36, No. 1, Jan.–Feb. 2013, pp. 240–249. doi:10.2514/1.56118

[16] Stevenson, D., and Schaub, H., "Multi-Sphere Method for Modeling Electrostatic Forces and Torques," *Advances in Space Research*, Vol. 51, No. 1, Jan. 2013, pp. 10–20. doi:10.1016/j.asr.2012.08.014

[17] Chow, P., Hughes, J., Bennett, T., and Schaub, H., "Automated Sphere Geometry Optimization for the Volume Multi-Sphere Method," *AAS/AIAA Spaceflight Mechanics Meeting*, AAS Paper 16-472, Springfield, VA, Feb. 2016, https://www.space-flight.org/docs/2016_winter/2016_winter.html.

[18] Ingram, G., Hughes, J., Bennett, T., Reily, C., and Schaub, H., "Volume Multi-Sphere-Model Development Using Electric Field Matching," *Journal of Astronautical Sciences*, Vol. 65, No. 4, 2018, pp. 377–399.

[19] Stevenson, D., and Schaub, H., "Optimization of Sphere Population for Electrostatic Multi-Sphere Model," *IEEE Transactions on Plasma Science*, Vol. 41, No. 12, 2013, pp. 3526–3535.

[20] Stevenson, D., "Remote Spacecraft Attitude Control by Coulomb Charging," Ph.D. Thesis, Univ. of Colorado, Boulder, CO, 2015.

[21] Harrington, R., *Field Computation by Moment Methods*, Wiley-IEEE, New York, 1968.

[22] Alad, R. H., and Chakrabarty, S., "Electrostatic Analysis of an Artificial Orbiting Satellite for Absolute Charging," *IEEE Transactions on Plasma Science*, Vol. 43, No. 9, Sept. 2015, pp. 2887–2893. doi:10.1109/TPS.2015.2454054

[23] Karthikeyan, B., Hariharan, V. K., and Sanyal, S., "Estimation of Free Space Capacitance and Body Potential of a Spacecraft for Charging Analysis," *IEEE Transactions on Plasma Science*, Vol. 41, No. 12, Dec. 2013, pp. 3487–3491. doi:10.1109/TPS.2013.2271280

[24] Chakrabarty, S., "Absolute Charging Analysis of Space-Craft Bodies Using Method of Moments (MOM)," *IEEE Applied Electromagnetics Conference (AEMC)*, IEEE Publ., Piscataway, NJ, 2015. doi:10.1109/AEMC.2015.7509140

[25] Mehta, P. D., and Chakrabarty, S. B., "Capacitance of Dielectric-Coated Metallic Bodies Isolated in Free Space," *Electromagnetics*, Vol. 31, No. 4, 2011, pp. 294–314. doi:10.1080/02726343.2011.568923

[26] Reitan, D. K., and Higgins, T. J., "Accurate Determination of the Accurate Determination of the Capacitance of a Thin Rectangular Plate," *Transactions of the American Institute of Electrical Engineers, Part I: Communication and Electronics*, Vol. 75, No. 6, 1957, pp. 761–766.

[27] Chow, Y., and Yovanovich, M., "The Shape Factor of the Capacitance of a Conductor," *Journal of Applied Physics*, Vol. 53, No. 8470, 1986, pp. 8470–8475.

[28] Schaub, H., and Jasper, L. E. Z., "Orbit Boosting Maneuvers for Two-Craft Coulomb Formations," *Journal of Guidance, Control, and Dynamics*, Vol. 36, No. 1, Jan.–Feb. 2013, pp. 74–82. doi:10.2514/1.57479

T. K. Minton
Associate Editor